Engineering synthetic agonists for targeted activation of Notch signaling

David H. Perez[1], Daniel Antfolk[1], Xiomar E. Bustos[1], Elliot Medina[1], Shiun Chang[1], Ahmed A. Ramadan[1], Paulo C. Rodriguez[1], David Gonzalez-Perez[1], Daniel Abate-Daga[1], Vincent C. Luca[1*]

[1] Department of Immunology, Moffitt Cancer Center, Tampa, FL 33602, USA
*Corresponding author, email: vince.luca@moffitt.org

ABSTRACT

Notch signaling regulates cell fate decisions and has context-dependent tumorigenic or tumor suppressor functions. Although there are several classes of Notch inhibitors, the mechanical force requirement for Notch receptor activation has hindered attempts to generate soluble agonists. To address this problem, we engineered synthetic Notch agonist (SNAG) proteins by tethering affinity-matured Notch ligands to antibodies or cytokines that internalize their targets. This bispecific format enables SNAGs to “pull” on mechanosensitive Notch receptors, triggering their activation in the presence of a desired biomarker. We successfully developed SNAGs targeting six independent surface markers, including the tumor antigens PDL1, CD19, and HER2, and the immunostimulatory receptor CD40. SNAGs targeting CD40 increase expansion of central memory γδ T cells from peripheral blood, highlighting their potential to improve the phenotype and yield of low-abundance T cell subsets. These insights have broad implications for the pharmacological activation of mechanoreceptors and will expand our ability to modulate Notch signaling in biotechnology.

INTRODUCTION

The Notch pathway is a cell-to-cell communication system that regulates embryonic development, tissue homeostasis, and immune cell differentiation. The signaling of mechanosensitive Notch receptors is tightly regulated[1] and aberrant Notch activity causes several human diseases[2]. For example, loss-of-function mutations in Notch components are linked to the development of aortic valve disease (Notch1), Alagille syndrome (Notch2, Jagged1), CADASIL (Notch3), spondylocostal dysostosis (DLL3)[3–6]. In cancer, Notch functions as a tumor suppressor or oncogene depending on the cell type, and both loss-of-function and hyperactivating mutations influence tumorigenesis and disease progression[7]. Notch is also pleiotropic with respect to its guidance of cell fate decisions, in that Notch activation stimulates either proliferation or differentiation in different stem

cell populations[8]. These diverse functions suggest that Notch agonists and antagonists may each be viable therapeutics in certain biomedical contexts[9].

The role of Notch in T cell biology has led to the development of several Notch-based strategies for enhancing cancer immunotherapy. Notch signaling is important for several natural stages of T cell maturation[10], and ex vivo Notch activation is required for the differentiation of T cells from hematopoietic stem cells (HSCs)[11]. This latter function may potentially be used to generate allogeneic T cells for “off-the-shelf” adoptive T cell or chimeric antigen receptor (CAR) T cell therapies. More recently, Notch activation has been shown to enhance the antitumor function of fully mature, activated T cells[12]. Genetic overexpression of an activated form of Notch[13], as well as culturing T cells in the presence of Notch1-specific antibodies[14] or ligand-expressing cells[15], were each associated with improved tumor clearance in various animal models of cancer. Detailed analysis of the T cells used in these studies revealed that these phenotypes were due to the Notch-stimulated induction of exhaustion-resistant or stem-like phenotypes.

At the molecular level, Notch receptors are massive (~290kD) transmembrane proteins that are activated by a distinctive, mechanical force-driven mechanism[16–18,1]. Notch signaling is initiated when a Delta-like (DLL) or Jagged (JAG) ligand forms a *trans*-interaction with a Notch receptor on the surface of an adjacent cell[1,19–21]. Endocytosis of the ligand then generates a “pulling” force that propagates to the negative regulatory region (NRR) of Notch [16,22]. This pulling destabilizes the NRR, which exposes internal cleavage sites for processing by the intramembrane proteases ADAM10 (S2 cleavage) and γ-secretase (S3 cleavage)[23,24]. Following these proteolytic events, the Notch intracellular domain (NICD) translocates to the nucleus to function as a transcriptional co-activator[25].

Although Notch inhibitors are widely available, the requirement for mechanical force in Notch activation has precluded the development of soluble agonists[9,18]. Specifically, these agents are challenging to engineer because they must somehow “pull” on the Notch receptor despite lacking a method of force generation. Several strategies have been developed to activate Notch receptors *in vitro* through mimicry of the physiological activation process. Notch signaling may be induced through co-culture of Notch-expressing cells and ligand-expressing cells, by culturing Notch-expressing cells on plates coated with ligands or antibodies, or by administration of ligand-coated microbeads[14,26,27]. By contrast, only a single antibody targeting Notch3, A13, has been reported to function as a soluble agonist[28]. Binding of this antibody promotes the unfolding of metastable

Notch3 NRR domains, which in turn exposes the S2 site for proteolytic cleavage [29]. Unfortunately, this NRR unfolding approach has been ineffective for receptor subtypes with stable NRRs (e.g., Notch1/2/4), and the lack of soluble agonists remains a significant void in our biochemical toolkit for manipulating the Notch pathway.

In this study, we engineered bispecific proteins that stimulate activation of Notch signaling in desired cellular contexts. We successfully developed SNAGs that enhance the signaling of weakly activating JAG1 ligands, as well as those that selectively activate Notch in the presence of the tumor biomarkers PDL1, CD19, and HER2. Furthermore, we show that SNAGs targeting the immunostimulatory receptor CD40 improve the expansion of γδ T cells from mixed cell populations. The modularity and versatility of this SNAG platform provide a blueprint for the development of a diverse repertoire of Notch-based biologics.

RESULTS

Soluble DLL4 ligand multimers do not activate Notch signaling. As an initial attempt to generate Notch agonists, we investigated whether soluble oligomers of an affinity-matured DLL4 ligand ($Delta^{MAX}$) activate Notch signaling[30]. $Delta^{MAX}$ contains ten mutations that increase its affinity for human Notch receptors by 500- to 1000-fold, making it a more potent activator than DLL4 in co-culture and plate-bound formats[30]. We hypothesized that this increased affinity, coupled with receptor crosslinking through multimerization, could introduce tension in the absence of an endocytic pulling force. To test this hypothesis, we incubated Notch1-Gal4 mCitrine reporter cells[31] with soluble and immobilized $Delta^{MAX}$ multimers (Fig. 1a-c). $Delta^{MAX}$ dimers were generated through the C-terminal addition of a dimeric human IgG1 Fc domain (Fig. 1b), and tetramers were generated by pre-mixing a 4:1 molar ratio of biotinylated $Delta^{MAX}$ with streptavidin (SA, Fig. 1c). We found that neither the monomers nor the multimers induced reporter activity. By contrast, the plated $Delta^{MAX}$ ligands potently stimulated Notch1 activation (Fig. 1a-c). This indicates that the receptor crosslinking by $Delta^{MAX}$-Fc dimers and $Delta^{MAX}$-SA tetramers is insufficient for signaling activation.

Design of synthetic Notch agonists. To develop soluble Notch agonists, we engineered bispecific proteins that recapitulate the endocytosis-linked activation mechanism of DLL and JAG ligands (Fig. 1d). SNAGs were created by fusing $Delta^{MAX}$ to the N-terminus of biomarker-targeting antibody fragments via a flexible $(GS)_5$ linker, or by fusing $Delta^{MAX}$ and antibody fragments to the N- and C-termini of a dimeric IgG1 Fc domain (Fig. 1e). These design concepts are intended to

103 form a “molecular bridge” between Notch-expressing cells and cells that express a given surface
104 protein. Conceptually, SNAGs should then activate Notch if the enforced interactions induce
105 endocytic or tensile force capable of unfolding the NRR.
106
107 **SNAGs rescue the signaling of a signaling-deficient DLL4 mutant.** To demonstrate proof-of-
108 concept, we tested whether SNAGs could rescue the activity of a signaling-deficient DLL4 mutant.
109 Loss-of-function DLL4 cells were generated by expressing a “headless” DLL4 truncation where
110 the Notch-binding C2 and DSL domains[20,32] were replaced with a BC2 epitope tag (BC2-DLL4^{HL})
111 (Fig. 2a, Fig. S1a)[33]. BC2-SNAGs were then generated by fusing Delta^{MAX} to a BC2-specific
112 nanobody (Figs. 2a-b, Fig. S2a). We found that BC2-DLL4^{HL} cells alone did not activate signaling
113 in a Notch1-Gal4 mCitrine reporter assay, whereas the addition of 1 nM to 100 nM concentrations
114 of SNAGs stimulated a dose-dependent increase in reporter activity (Fig. 2c, Fig. S3a-c).
115 Monomeric BC2-SNAGs containing the $(GS)_5$ linker (BC2-SNAG) stimulated a ~6-fold increase
116 in Notch1 signaling, whereas dimeric BC2-SNAG Fc fusion proteins (BC2-SNAG^{Fc}) were more
117 effective and induced a ~10-fold increase (Fig. 2c). Importantly, administration of the monomeric
118 or dimeric BC2-SNAGs alone did not substantially increase Notch1 reporter activity, indicating
119 that a mixture of target-expressing and non-expressing cells is required for SNAG-mediated
120 activation (Fig. 2c).
121
122 **SNAGs bolster the activity of weakly-signaling JAG1 ligands.** DLL or JAG ligands
123 preferentially signal through certain Notch receptor subtypes, and JAG1 is a particularly weak
124 activator of Notch1[34]. Therefore, we tested whether a JAG1-targeting SNAG (JAG1-SNAG^{Fc})
125 could potentiate JAG1-Notch1 signaling. In the JAG1-SNAG^{Fc} construct, Delta^{MAX} and an scFv
126 derived from the JAG1-targeting antibody B70[35] were fused to the N- and C-termini of an IgG1 Fc
127 domain as described above (Fig. S2b). We then performed a signaling assay to measure the
128 activation of Notch1 reporter cells by JAG1-overexpressing HEK293 cells (JAG1-293 cells) in the
129 presence or absence of the SNAG. We found that addition of the JAG1-SNAG^{Fc} increased Notch1
130 reporter activity by ~4-fold compared to JAG1-293 cells alone, and that JAG1-293 cells did not
131 stimulate a significant increase in reporter activity (Fig. 2d, Fig. S1b). We also evaluated the
132 JAG1-SNAG^{Fc} with a JAG1 H268Q “Nodder” mutant that causes Alagille syndrome-like symptoms
133 in mice by decreasing JAG1-Notch1 binding (Fig. S1c). Addition of the JAG1-SNAG^{Fc} to
134 cocultures of Notch1 and JAG1^{H268Q} cells increased JAG1 signaling by up to 7-fold compared to
135 JAG1^{H268Q} cells alone (Fig. 2e). These data indicate that SNAGs can function as “signaling
136 enhancers” by potentiating the activity of endogenous or mutated ligands.

137

138 **SNAGs targeting tumor antigens activate Notch in mixed cell populations.** We next tested
139 whether SNAGs targeting the tumor antigens PD-L1, CD19, or HER2 (Fig. 3a) can stimulate
140 Notch activation. There is mounting evidence that Notch signaling enhances the function of
141 activated T cells[13–15], and SNAGs localized to the tumor microenvironment have the potential to
142 stimulate localized activation of tumor-associated lymphocytes. For these SNAGs, the targeting
143 arms were derived from antibody-drug conjugates (ADCs) that were pre-selected for their ability
144 to induce target internalization. We hypothesized that SNAGs incorporating ADC antibodies could
145 thus mimic the physiological endocytosis mechanism of DLL or JAG ligands.

146

147 We generated monomeric and dimeric PDL1-SNAGs by fusing Delta^{MAX} to a single-chain variable
148 fragment (scFv) derived from the ADC antibody Atezolizumab[36,37]. In the monomeric PDL1-SNAG,
149 Delta^{MAX} and the scFv were connecting using a $(GS)_5$ linker, and in the dimeric PDL1-SNAG
150 (PDL1-SNAG^{Fc}), Delta^{MAX} and the scFv were fused to the N- and C-termini of an IgG1 Fc domain
151 (Fig. 3a, Fig. S2a). Unexpectedly, addition of the monomeric PDL1-SNAG to a 1:1 mixture of
152 Notch1 reporter cells and PDL1-expressing MDA-MB-231 cells did not activate Notch1 (Fig. 3b,
153 Fig. S1d). However, the dimeric PDL1-SNAG^{Fc} protein stimulated a ~7-fold increase in Notch1
154 signaling in the coculture, suggesting that multimerization or avidity-enhancement may be
155 required for SNAGs to effectively target biomarkers other than Notch ligands (Fig. 3b). Neither
156 the PDL1-SNAG nor the PDL1-SNAG^{Fc} substantially increased Notch1 reporter activity in the
157 absence of MDA-MB-231 cells. Because of the increased efficacy of the dimeric SNAGs (Fig. 2c,
158 Fig. 3b), we designed subsequent CD19- and HER2-SNAGs using only the Fc-fusion format (Fig.
159 3a).

160

161 **SNAGs do not activate signaling on cells expressing both Notch1 and PD-L1.** Given the
162 ubiquitous expression of Notch1 in mammalian cells, it is conceivable that SNAGs could activate
163 signaling when Notch1 and the target protein are both present on the cell surface. To test this
164 possibility, we cultured MDA-MB-231 cells in the presence of soluble Delta^{MAX}-Fc, PDL1-SNAG^{Fc},
165 or immobilized Delta^{MAX}-Fc and monitored the levels activated Notch1 by Western Blot (Fig. 3c).
166 We found that the plated Delta^{MAX}-Fc protein stimulated high levels of Notch1 activation, whereas
167 the PDL1-SNAG^{Fc} did not induce signaling over the background levels observed for soluble
168 Delta^{MAX}-Fc alone (Fig. 3c). The inability of SNAGs to activate Notch1 in MDA-MB-231 cells
169 suggests that the present design does not enable sufficient intercellular crosslinking in cultures of
170 cells expressing both Notch1 and the biomarker.

171

172 **Development of SNAGs targeting CD19 and HER2.** To generate a SNAG targeting the B-
173 lymphocyte antigen CD19, we fused an scFv derived from the CD19-targeting ADC
174 loncastuximab[38] to the C-terminus of Delta^{MAX}-Fc (CD19-SNAG^{Fc}, Fig. S2a). The CD19-SNAG
175 was then added to Notch1 reporter cells or to co-cultures of Notch1 reporter cells and CD19-
176 overexpressing 3T3 fibroblast cells (Fig. S1e). We found that the CD19-SNAG^{Fc} protein stimulated
177 up to a 6-fold increase in reporter activity in the co-culture compared to untreated Notch1 cells
178 (Fig. 3d). To generate a SNAG targeting the breast cancer antigen HER2 (HER2-SNAG^{Fc}), we
179 replaced the CD19-targeting arm with an scFv derived from the HER2-targeting ADC
180 trastuzumab[39] (Fig. S2c). Addition of the HER2-SNAG^{Fc} to a mixed culture of Notch1 reporter cells
181 and HER2-expressing SK-BR-3 breast cancer cells induced a 6-fold increase in reporter activity
182 (Fig. 3e, Fig. S1f) at the highest concentration tested (100 nM), which is similar to the level of
183 activation we observed for the PDL1-SNAG^{Fc} and the CD19-SNAG^{Fc} constructs (Fig. 3b, 3d). In
184 the absence of biomarker-expressing cells, neither the CD19-SNAG^{Fc} nor the HER2-SNAG^{Fc}
185 stimulated a significant increase in signaling compared to Delta^{MAX}-Fc alone (Fig. 3d-e). Our
186 collective development of PD-L1, CD19, and HER2 SNAGs demonstrates that SNAGs can
187 facilitate signaling by engaging cell surface proteins beyond endogenous ligands.

188

189 **Endocytosis is required for SNAG-mediated Notch activation.** Ligand endocytosis is
190 important for Notch activation[40], and this process is regulated by ubiquitination of DLL or JAG
191 ICDs by the E3 ligase Mindbomb1[41–43]. To determine whether endocytosis occurs with a SNAG
192 targeting a surface protein other than a natural Notch ligand, we performed an immunofluorescent
193 endocytosis assay utilizing CD19-SNAG^{Fc} in CD19-expressing cells. CD19-SNAG^{Fc} coupled with
194 a fluorescent secondary antibody (Alexafluor 647-labeled anti-Fc) bound strongly to the surface
195 of the CD19-expressing cells when the mixture was incubated on ice (Fig 4a, Fig. S4a-c), and the
196 contours of the cells were identified by staining for filamentous actin (Fig. S4a). Incubating the
197 cells at 37 °C after attaching CD19-SNAG^{Fc}-647 to cells allowed for cellular functions, including
198 endocytosis, to resume. Visualizing the cells after a 15 min incubation at 37 °C showed that the
199 majority of CD19-SNAG^{Fc} is internalized (Fig. 4b, Fig. S4e-d).

200

201 To test whether endocytosis is necessary for SNAG function, we co-administered SNAGs with the
202 dynamin-dependent endocytosis inhibitor Dynasore. We found that Dynasore completely ablated
203 the activity of CD19-SNAG^{Fc} in co-cultures of Notch1- and CD19-expressing cells, indicating that
204 endocytosis is required for SNAG-mediated activation utilizing CD19 as a biomarker (Fig. 4c). We

205 further found that BC2-SNAGs targeting BC2-DLL4^{HL} were unable to activate Notch1 in co-
206 cultures of Notch1 and BC2-DLL4^{HL} cells in the presence of Dynasore, confirming that
207 endocytosis is also required for SNAG-mediated rescue of DLL4 signaling (Fig 4d-e.)
208 Interestingly, we found that immobilized SNAGs were also unable to activate Notch1 in the
209 presence of Dynasore, suggesting that endocytosis in the Notch-receptor cell is essential for
210 Notch activation by plated ligands (Fig. 4f). These studies demonstrate that Notch activation by
211 plated ligands, SNAGs targeting a DLL4 loss-of-function mutant, and SNAGs targeting tumor
212 antigens each depend on endocytosis. However, it is currently unclear whether endocytosis of
213 the receptor, ligand, or both, is essential for SNAG function.
214
215 **SNAGs targeting CD40L increase the expansion of γδ T cells.** We next generated a SNAG
216 targeting CD40 (CD40-SNAG), an immunostimulatory receptor that undergoes endocytosis upon
217 binding to CD40 ligand (CD40L)[44]. We hypothesized that a CD40-SNAG could be used to activate
218 Notch in T cells in the presence of CD40^{+} B cells, as these cell types are known to colocalize in
219 germinal centers, peripheral blood, the tumor microenvironment, and other biological contexts[45].
220 To generate a CD40-SNAG, we fused Delta^{MAX} and the ECD of CD40L to the N- and C-termini of
221 a trimeric leucine zipper[46] (Fig. 5a, Fig. S2d), respectively. This trimeric scaffold was selected
222 instead of an Fc domain for the CD40-SNAG because CD40L is naturally a homotrimer. We found
223 that addition of the CD40-SNAG robustly activated Notch in mixed cultures of Notch1 reporter
224 cells and CD40-expressing OCI-Ly3 cells (Fig. S1g), but only weakly in Notch1 reporter cells
225 alone (Fig. 5b). Notably, OCI-Ly3 cells used in this assay are non-adherent, indicating that SNAGs
226 may facilitate Notch activation between adherent cells and those grown in suspension.
227
228 There has been a growing interest in γδ T cell-based cancer immunotherapies, including the
229 adoptive transfer of unmodified γδ T cells and the development of γδ T CAR T cells[47–49]. It was
230 previously shown that Notch1 and Notch2 are important for γδ T cell antitumor function[50], and that
231 Notch stimulation generally induces memory phenotypes in mature and activated T cells[15,14].
232 Therefore, we sought to determine whether the CD40-SNAG could be used to improve the
233 expansion and phenotype of γδ T cells isolated from peripheral blood mononuclear cells
234 (PBMCs). To determine the ratio of CD40-expressing and non-expressing cells, we analyzed
235 PBMCs by flow cytometry. We found that a representative PBMC culture contained 18.6% CD19+
236 CD40^{+} B cells and 71.9% CD3^{+} CD40^{-} T cells (Fig. 5c), suggesting that the T cell fraction would
237 be amenable to stimulation with the CD40-SNAG.
238

239 To test the effect of the CD40-SNAG on γδ T cells, we administered increasing amounts of CD40-
240 SNAG during an established γδ T cell expansion protocol[51]. Addition of the CD40-SNAG
241 increased both the relative amount and total amount of γδ T cells recovered at all concentrations
242 tested (Fig. 6a-c). We found that the highest CD40-SNAG concentration (500 ng/mL) was
243 associated with >4-fold increase in the total number of γδ T cells compared to untreated PBMCs
244 or those treated with Delta^{MAX}-Fc or trimerized CD40L alone. Treatment with 500 ng/mL CD40-
245 SNAG also induced a ~4-fold increase in the number of central memory cells and a significant
246 reduction in the number of effector memory γδ T cells (Fig. 6d). This bias towards the central
247 memory subset is a desirable outcome given that central memory T cells have increased survival
248 and antitumor function compared with effector memory T cells and effector T cells[52].
249
250 **DISCUSSION**
251 The development of soluble agonists has been an enduring challenge in the Notch field[9,53]. The
252 SNAG platform described here offers a solution to this problem and provides a framework for the
253 development of a diverse array of Notch activating biologics. Such agents have a wide range of
254 potential translational applications, particularly in cancers where Notch functions as a tumor
255 suppressor[7], T cell manufacturing[11,27], T cell immunotherapy[13–15], wound healing[54], and other
256 areas of regenerative medicine. These first-generation SNAGs were engineered using an Fc-
257 fusion format used in clinically viable protein drugs, which may also help to accelerate *in vivo*
258 translation.
259
260 In their present form, SNAGs facilitate potent activation of Notch signaling in mixed populations
261 of cells. However, we anticipate that the design may be tuned to further optimize SNAG function.
262 For example, it may be preferable to engineer SNAGs such that the target binding arm has a
263 higher binding affinity than the Notch-binding arm to improve specificity and tissue distribution.
264 Such strategies have been successfully employed both for bispecific inhibitory antibodies[55] and T
265 cell engagers[56]. Additionally, higher-order oligomers beyond the dimeric and trimeric SNAG
266 scaffolds tested here may lead to increased signaling potency. Future studies will focus on
267 optimizing affinity and multimerization to maximize signaling while maintaining favorable
268 biochemical properties.
269
270 One surprising observation was that PDL1-SNAGs did not activate signaling on cells expressing
271 both PDL1 and Notch1. We speculate that these SNAGs engage the two targets in *cis* on the
272 surface of a single cell, as opposed to bridging PDL1 and Notch1 proteins between cells, and that

273 *cis* interactions do not introduce sufficient tension to unfold the NRR. This may be attributed to
274 the restricted diffusion of SNAGs in the 2-dimensional environment of the membrane, which can
275 promote preferential *cis* interactions by increasing the local concentration. Previous studies have
276 shown that *cis* inhibition of Notch signaling occurs when ligands and receptors are expressed on
277 the same cell[31,57], and it appears that SNAGs are similarly unable to activate Notch in this context.
278 Regardless, the ability of SNAGs to mediate unidirectional signaling enables highly selective
279 targeting, which could minimize the risks of potential toxicity from global Notch agonism.
280
281 There has been a longstanding interest in using Notch stimulation to manufacture "off-the-shelf"
282 $CD4^+$ or $CD8^+$ T cells for immunotherapy[58]. By contrast, the field of γδ T cell immunotherapy
283 emerged more recently and the role of Notch in their biology is less thoroughly understood[47].
284 These cells represent only 1-10% of the T cell population in healthy donors, and protocols for the
285 manufacture of pure populations of functional γδ T cells are continuously being optimized[59,60]. We
286 showed that the addition of a CD40-SNAG can greatly increase both the total number of γδ T
287 cells and the fraction of cells with desirable central memory phenotypes. This expansion was not
288 observed upon the addition of trimerized CD40L, suggesting that CD40 signaling alone is not able
289 to recapitulate the effects of the CD40-SNAG. In future studies, it will be interesting to probe
290 whether Notch stimulation in γδ T cells is associated with enhanced antitumor function akin to
291 what is observed for conventional activated T cells[14], or whether there are synergistic effects
292 between Notch activation in T cells and CD40 activation in B cells.
293
294 Although SNAGs are effective in mixed cell populations, the development of "unconditional"
295 agonists that do not rely on a secondary target remains a challenging problem. Thus far, it appears
296 that the metastable NRR of Notch3 is uniquely susceptible to antibody-mediated
297 destabilization[29,61]. The engineering of agonists targeting other Notch receptors with more stable
298 NRRs may require alternative solutions. The successful activation of Notch1 with ligands
299 immobilized on beads[27] or DNA origami structures[62] suggests that oligomerization may be an
300 effective strategy, but these methods are not currently viable for in vivo applications. Despite these
301 limitations, the development of SNAGs represents a key first step towards the widespread
302 development of Notch activating molecules for basic and translational research.
303
304 **AUTHOR CONTRIBUTIONS**
305 V.C.L. and D.H.P. wrote the manuscript. V.C.L., D.H.P, D.A., and D.A.D. designed the
306 experiments. D.H.P. cloned the SNAG constructs, purified the proteins, and performed the

signaling assays. E.M. and D.G.P. generated the Delta^{MAX} constructs. D.A. performed the Notch activation assays in MDA-MB-231 cells and immunofluorescent endocytosis assays. X.E.B. performed T cell expansion assays. P.C.R. and S.C. assisted with immunology experiments. V.C.L. supervised the project and edited the manuscript.

ACKNOWLEDGEMENTS.

This project was supported by NIH R35GM133482 (V.C.L. and D.A.), the Sigrid Juselius Foundation (D.A.) and NIH R35 Diversity Supplement R35GM133482-03S2 (E.M.). V.C.L. is a Rita Allen Scholar. Shared resources were provided by the Moffitt Cancer Center Support Grant NIH P30CA076292.

COMPETING INTERESTS

V.C.L. is a consultant on unrelated projects for Cellestia Biotech, Remunix, and Curie.Bio. The remaining authors have no competing interests. V.C.L. and D.H.P. have filed provisional patents (serial numbers 63/548,615 and 63/663,744) based on the described technology.

FIGURES AND FIGURE LEGENDS

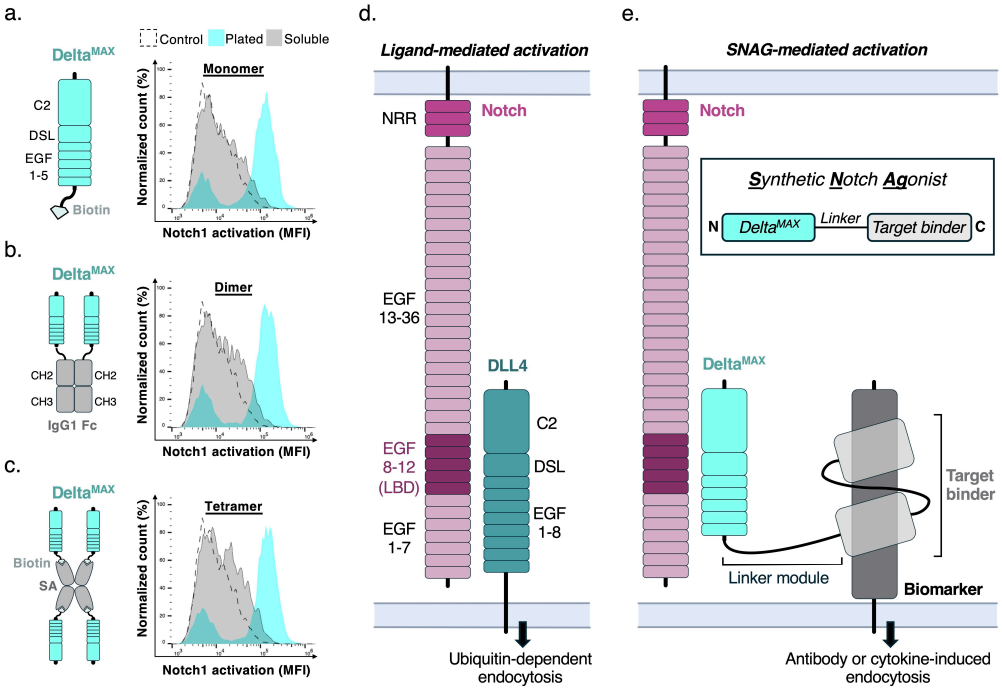

Figure. 1. Design concept for synthetic Notch agonists. (a) Flow cytometry histogram overlay of Notch1 reporter cells stimulated by soluble or plated (non-specifically adsorbed) Delta^{MAX}. The cartoon depicts the site-specifically biotinylated Delta^{MAX}(N-EGF5) construct. (b) Histogram overlay of Notch1 reporter cells stimulated with soluble or plated Delta^{MAX}-Fc protein. (c) Histogram overlay of Notch1 reporter cells stimulated with plated or soluble Delta^{MAX}-SA tetramers. (d) Cartoon schematic depicting the ECDs of Notch1 and DLL4 interacting during canonical Notch activation. The NRR and ligand-binding domains (LBD) of Notch1 (EGF domains 8-12) are shaded. (e) Schematic of a generalized SNAG construct alongside a cartoon depicting SNAG-mediated Notch activation.

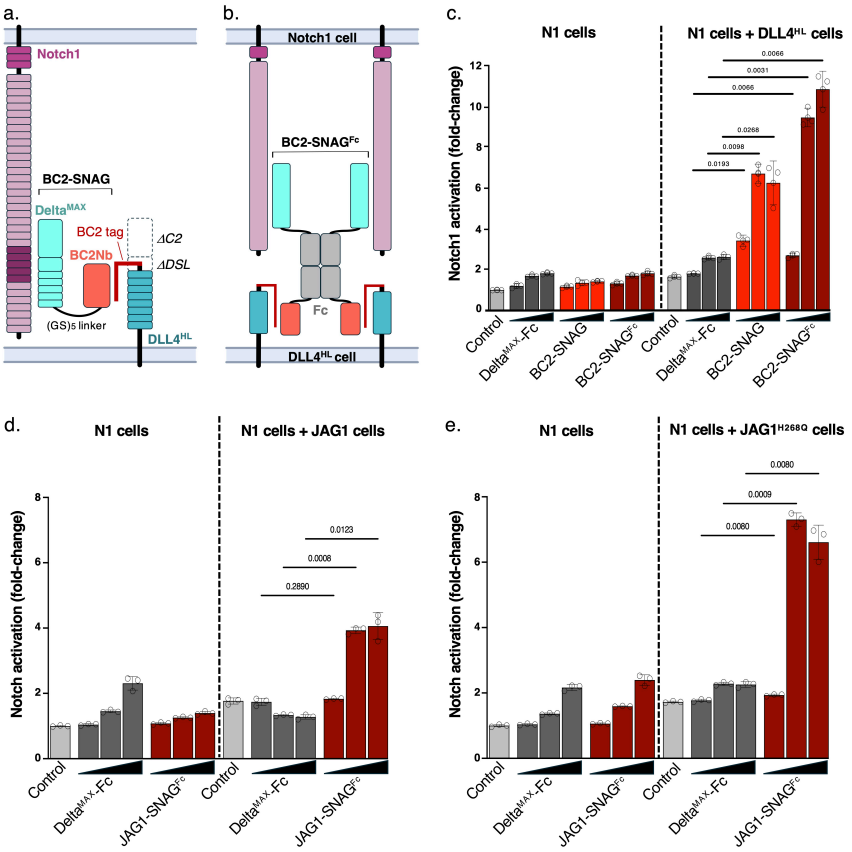

Figure. 2. SNAGs rescue the signaling of binding-deficient DLL4 and JAG1 mutants. (a) Cartoon schematic depicting a SNAG binding to Notch1 and a loss-of-function DLL4 mutant. The "headless" loss-of-function DLL4 protein ($DLL4^{HL}$) was generated by replacing the Notch-binding C2-DSL region with a BC2 peptide epitope recognized by the anti-BC2 nanobody. (b) Cartoon schematic depicting the multivalent binding of a dimeric Fc-tagged SNAG ($BC2\text{-}SNAG^{Fc}$) to Notch1 and "headless" DLL4. (c-e) Fluorescent reporter assays were used to evaluate SNAG-mediated activation of Notch1 in cocultures with HEK293T cells expressing $DLL4^{HL}$ (c), JAG1 (d), or $JAG1^{H268Q}$ (e). Increasing concentrations (1 nM, 10 nM, or 100 nM) of the indicated SNAGs were added to Notch1-Gal4 Citrine reporter cells alone, or to a 1:1 mixture of Notch1 reporter cells and HEK293 cells expressing $DLL4^{HL}$, and fluorescence was measured by flow cytometry. A representative experiment from three biological replicates is shown. Mean fluorescence intensity (MFI) was normalized to the mean MFI of Notch1 reporter cells alone. Error bars represent the standard deviation of three technical replicates with the *P* value by Student's *t* test shown above each comparison.

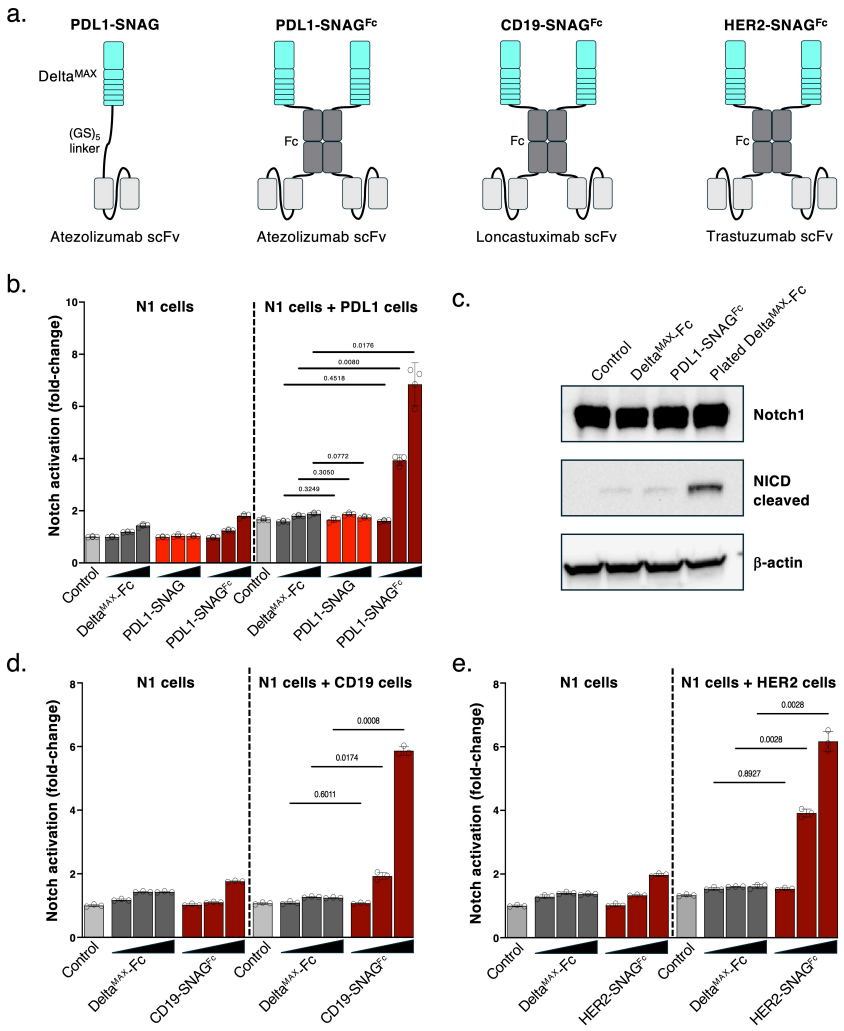

Figure. 3. SNAGs targeting tumor antigens activate Notch in mixed cell populations. (a) Cartoon schematics of PDL1, CD19, and HER2 SNAGs. (b) PDL1-SNAG-mediated activation of Notch1 was evaluated in a fluorescent reporter assay. Increasing concentrations (1 nM, 10 nM, or 100 nM) of Delta^{MAX}-Fc, PDL1-SNAG, or PDL1-SNAG^{Fc} were added to Notch1-Gal4 mCitrine reporter cells alone, or a 1:1 mixture of Notch1 reporter cells and MDA-MB-231 cells. (c) Activation of Notch1 in MDA-MB-231 cells, which express both PDL1 and Notch1, was assessed by Western Blot using an antibody against the activated NICD. (d, e). Notch1 activation by CD19-SNAGs and HER2-SNAGs, was evaluated using a fluorescent reporter assay. Increasing concentrations (1 nM, 10 nM, or 100 nM) of Delta^{MAX}-Fc or each SNAG^{Fc} were added to Notch1-Gal4 mCitrine reporter cells alone, or a 1:1 mixture of Notch1 reporter cells and CD19-overexpressing 3T3 cells (d) or HER2-expressing SK-BR-3 cells (e). For b, d, and e, a representative experiment from three biological replicates is shown. Mean fluorescence intensity (MFI) was normalized to the mean MFI of Notch1 reporter cells alone. Error bars represent the standard deviation of three technical replicates with the *P* value by Student's *t* test shown above each comparison.

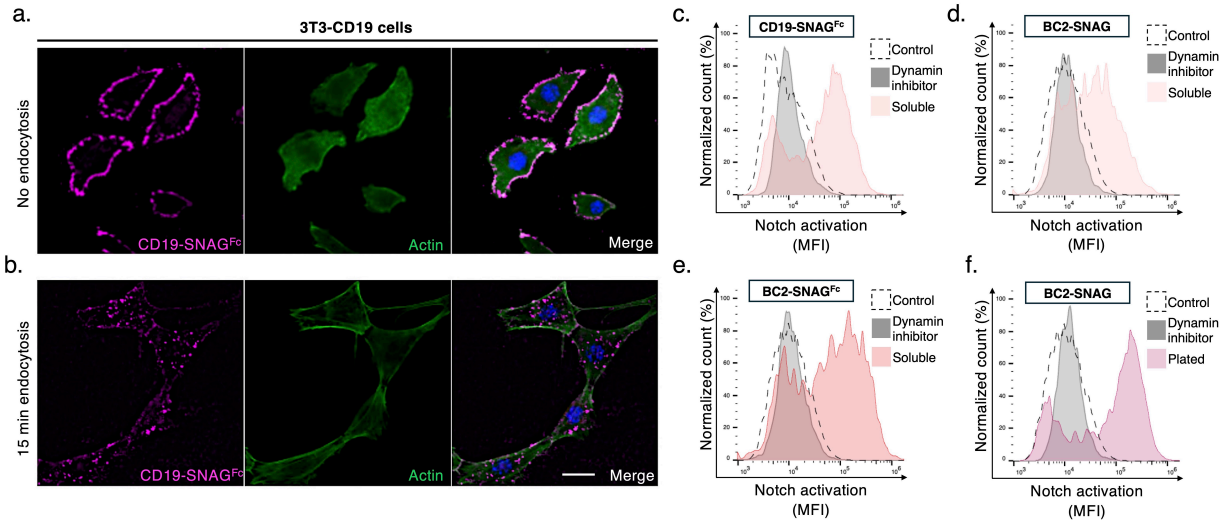

Figure 4. SNAG-mediated Notch activation requires endocytosis. (a) Representative immunofluorescence images of fluorescently labeled CD19-SNAGs (magenta) used to stain the surface of CD19 expressing 3T3 cells that were kept on ice. CD19-SNAGs visualized by Alexa Fluor anti-Fc 647. To visualize the contours of the cells, the actin cytoskeleton was stained using phalloidin-488 (green). Nuclei counterstained by Hoechst 33342 (blue). Scale, 20 mm. (b) Representative immunofluorescence images of fluorescently labeled CD19-SNAGs used to stain the surface of CD19 expressing 3T3 cells, followed by washing away unbound SNAGs and subjecting the cells to a 15 min incubation in a 37 ºC incubator to resume cellular processes including endocytosis. After 15 min the cells were fixed and stained in parallel with the no endocytosis samples. Scale, 20 mm. (d-e) Flow cytometry histogram overlays depicting Notch1 reporter activity induced by soluble CD19-SNAG^{Fc}, BC2-SNAG, or BC2-SNAG^{Fc} in the presence or absence of Dynasore. (c) Notch1 reporter cells were co-cultured with CD19-overexpressing 3T3 cells. In (d) and (e), Notch1 reporter cells were co-cultured with HEK293 cells expressing DLL4^{HL}. (f) Flow cytometry histogram overlay depicting Notch1 reporter activity induced by immobilized BC2-SNAG in the presence or absence of Dynasore. A representative histogram is shown for each experimental condition from one of three biological replicates.

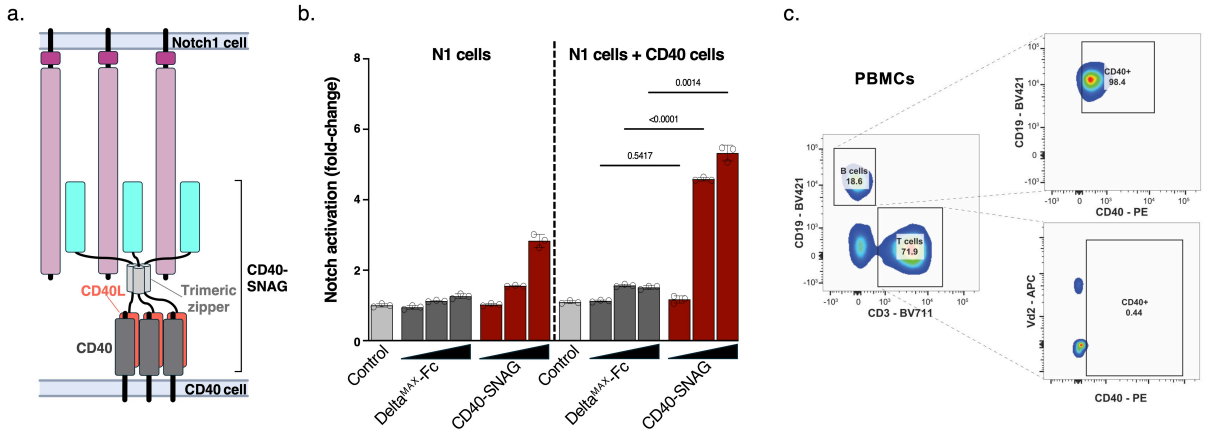

Figure 5. Trimeric CD40-SNAGs activate Notch1 signaling. (a) Cartoon schematic depicting a SNAG binding to Notch1 and CD40 receptor on adjacent cell. The CD40-SNAG was generated by using a GCN4 leucine zipper to trigger dimerization of both the Notch1- and CD40-targeting domains. (b) A fluorescent reporter assay was used to evaluate SNAG-mediated activation of Notch1. Increasing concentrations (1 nM, 10 nM, or 100 nM) of Delta^{MAX}-Fc or CD40-SNAG were added to Notch1-Gal4 mCitrine reporter cells alone or a 1:2 mixture of Notch1 reporter cells and OCI-Ly3 cells that have high expression of the CD40 receptor and fluorescence was measured by flow cytometry. A representative experiment from three biological replicates is shown. Mean fluorescence intensity (MFI) was normalized to the mean MFI of Notch1 reporter cells alone. Error bars represent the standard deviation of three technical replicates with the *P* value by Student's *t* test shown above each comparison. (c) Flow cytometry plots showing the percentage of B cells and T cells on a healthy donor sample, gated on lymphoid, single, live cells. The percentage of CD40+ cells in the B cell subpopulation (CD19+) are shown in the top panel, and the T cell subpopulation (CD3+) on shown in the bottom panel.

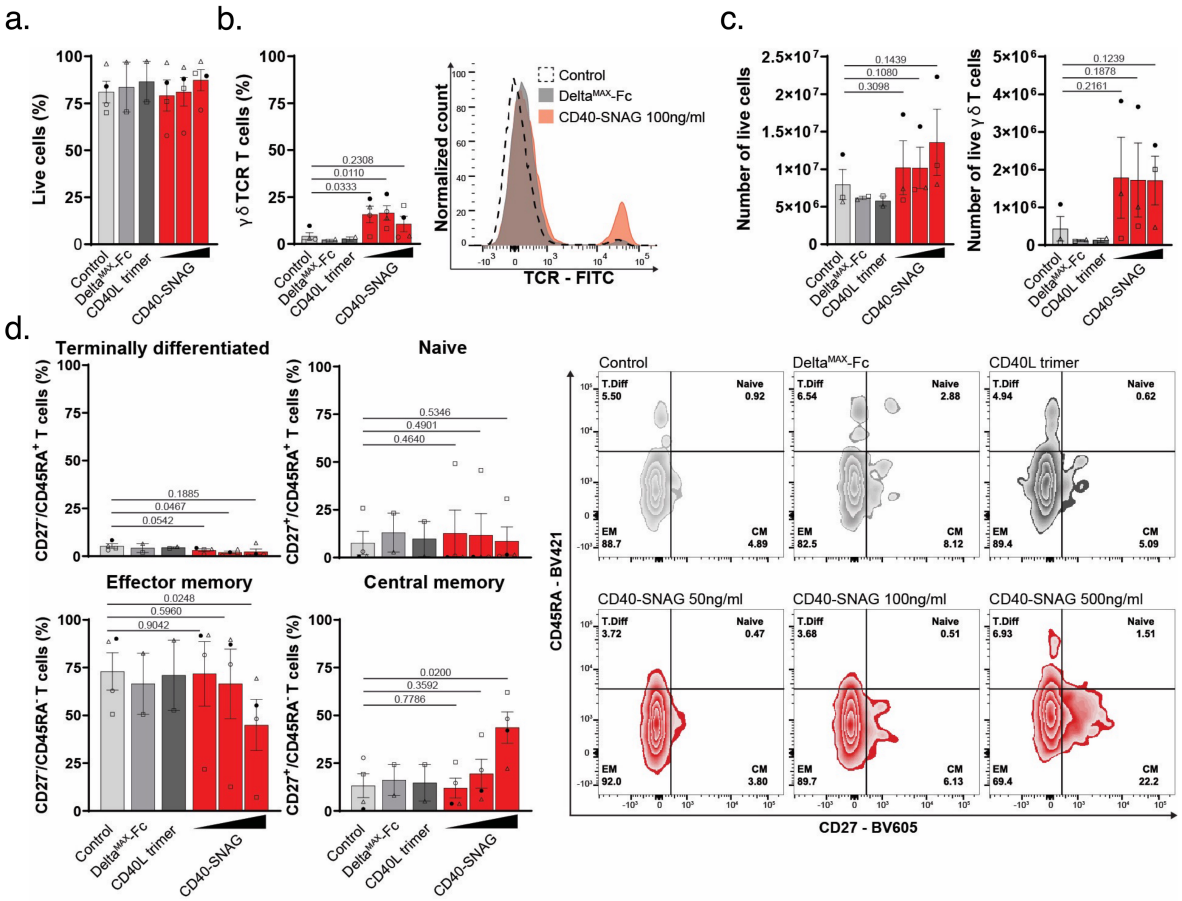

Figure. 6. CD40-SNAGs improve the expansion and phenotype of γδ T cells. (a) Bar chart showing the percentage of live cells in culture with different concentrations of CD40-SNAG or controls; gated on lymphoid, single cells. (b) Percentage of γδ TCR expression in T cells cultured with CD40-SNAG vs controls. The histogram to the right shows data from a representative biological replicate; gated on lymphoid, single, viable, CD3+ cells. (c) Bar graph showing the total number of cells in culture by each condition (left) and the relative number of γδ TCR^+ cells (right). (d) Bar charts representing the distribution of different differentiation phenotypes in γδ TCR^+ T cells cultured with CD40-SNAG or controls. A representative flow cytometry zebra plot from one healthy donor is shown to the right. Cells were analyzed and counted on day seven, in the bar charts each symbol correspond to an independent donor (biological replicate), p values over the bars were calculated using paired t-tests comparing to the control.

433 **MATERIALS AND METHODS**

434 **Protein expression and purification**

435 All SNAG sequences were cloned into a pAcGP67A vector for insect cell production containing
436 an N-terminal gp67 signal peptide and C-terminal 8xHis-tag. Monomeric SNAGs were generated
437 by fusing a truncated version of the Delta^{MAX} protein spanning from the N-terminus to EGF5 (N-
438 EGF5) fused to a biomarker-targeting scFv or nanobody using a flexible $(GS)_5$ linker. Dimeric
439 SNAG^{Fc} constructs were generated by fusing Delta^{MAX} (N-EGF5) and the biomarker targeting
440 module to the N- and C-termini of a human IgG1 Fc domain, respectively. All SNAG^{Fc} constructs
441 contained short GSG-linkers between the Fc sequence and Delta^{MAX} or the targeting module.
442 Published sequences of atezolizumab, trastuzumab, and loncastuximab[63] were converted into a
443 scFv format prior to being incorporated into SNAGs, and the sequence of the BC2-specific
444 nanobody[33] was obtained from the Protein Data Bank (PDB ID 5VIN). Each scFv was generated
445 by fusing the C-terminus of the variable heavy (V_H) domain to the N-terminus of the variable light
446 (V_L) domain with a $(GGGGS)_3$ linker. Biotinylated Delta^{MAX}(N-EGF5) protein was generated
447 through enzymatic modification of a C-terminal biotin acceptor peptide (BirA tag) as previously
448 described[30]. The "headless" loss-of-function DLL4^{HL} mutant was generated by replacing the C2
449 and DSL domains of human DLL4 with the BC2-peptide sequence, which was connected to the
450 N-terminus of EGF1 by a short GSG-linker. The DLL4^{HL} construct was cloned into a pLenti-IRES-
451 Puro vector for mammalian expression.

452

453 All SNAG constructs in this study were expressed for by infecting *Trichoplusia ni* insect cell
454 cultures (Expression Systems) at a density of 2×10^6 cells ml^{-1} with recombinant Baculovirus.
455 Culture supernatants were harvested after 48h, and proteins were purified by nickel and size-
456 exclusion chromatography. Biotinylated proteins were site-specifically modified using BirA ligase
457 and excess biotin was removed by purifying the proteins on a size-exclusion column. Protein
458 purity was assessed by SDS–PAGE using TGX 12% Precast gels (Bio-Rad). All proteins were
459 flash-frozen in liquid nitrogen and stored at −80 °C following purification.

460

461 **Cell culture and generation of cell lines**

462 Mammalian cells were cultured at 37 °C, with a humidified atmosphere of 5% CO2, washed with
463 Dulbecco's PBS (DPBS, Corning), and detached with trypsin–EDTA 0.25% (Gibco) for
464 subculturing or cell-based assays. Notch reporter cell lines CHO-K1 N1-Gal4 were a gift from Dr.
465 Michael Elowitz (California Institute of Technology)[31]. Briefly, transfections of HEK293T cells were
466 carried out with packaging vectors VSV-G and d8.9 in the presence of polyethyleneimine at a ratio

467 of 4:1 (DNA:polyethyleneimine). HER2^{+} SK-BR-3 cells, human CD19-overexpressing 3T3 cells,
468 PD-L1^{+} MDA-MB-231, and CD40^{+} OCI-Ly3 cells were gifts from Drs. Brian Czerniecki, Fred
469 Locke, Eric Lau, and John Cleveland, respectively (Moffit Cancer Center). HEK293T, SK-BR-3,
470 3T3 mouse fibroblast, and MDA-MB-231 cells were cultured in high-glucose DMEM (Cytiva)
471 supplemented with 10% FBS (peak serum) and 2% penicillin/streptomycin (Gibco). Puromycin
472 5 μg ml^{-1} was added to HEK293T cell cultures to maintain homogeneous populations of receptor-
473 expressing cells. CHO-K1 N1-Gal4 cells were cultured in minimum essential medium Eagle-alpha
474 modification (α-MEM, Cytiva) supplemented with 10% FBS (peak serum), 2%
475 penicillin/streptomycin (Gibco), 400 μg ml−1 of zeocin (Alfa aesar) and 600 μg ml−1 of geneticin
476 (Gibco). Expression of receptors on the cell surface was confirmed by flow cytometry (BD Accuri
477 C6 plus) staining the cell lines with anti-hDLL4 PE, anti-JAG1 APC, anti-hPDL1 FITC, anti-hHER2
478 (anti-IgG FITC), anti-hCD19 FITC, and anti-CD40 PE in DMEM supplemented with 10% FBS for
479 1 h at 4 °C.
480
481 **Notch activation with Delta^{MAX} multimers**
482 On day one, biotinylated Delta^{MAX}, Delta^{MAX} tetramers formed with streptavidin, or Delta^{MAX}-Fc
483 were reconstituted in DPBS and adsorbed to tissue culture 96-well plates (Costar) for 1 h at 37 °C.
484 The wells were then washed three times with 200 μl of DPBS to remove unbound proteins. Next,
485 CHO-K1 N1-Gal4 cells were detached with trypsin–EDTA 0.25% (Gibco) and manually counted.
486 Appropriate dilutions were prepared in α-MEM media to ensure 30,000 CHO-K1 N1-Gal4 cells
487 per well in a volume of 50 mL. Cells were transferred to the ligand-coated plates and cultured for
488 24 h at 37 °C in 5% CO2. On day two, CHO-K1 N1-Gal4 cells were washed with 200 μl DPBS,
489 detached with 30 μL of trypsin–EDTA 0.25%, and quenched with 170 mL of α-MEM media. Finally,
490 cells were resuspended, and the H2B-mCitrine signal was measured by flow cytometry (BD Accuri
491 C6 plus). CHO-K1 N1-Gal4 cells alone were used as the control. The measurements represent
492 the mean fluorescent intensity as fold-change of Notch activation ± s.d. of three technical
493 replicates. Notch activation was normalized to wells containing CHO-K1 N1-Gal4 cells alone.
494
495 **Notch activation with SNAGs in coculture of cells expressing the target tumor biomarker**
496 On day one, cells expressing the target receptor of the SNAG (signal-sending cells) were
497 detached with trypsin–EDTA, counted manually, and dilutions prepared such that 50 mL of DMEM
498 containing 15,000 signal-sender cells were added to wells of a tissue culture 96-well plate. The
499 next day, CHO-K1 N1-Gal4 reporter cells (signal-receiver cells) were detached with trypsin–
500 EDTA, and 50 μl of α-MEM media containing 30,000 cells were added to the tissue culture 96-

501 well plate containing the signal-sending cells after combining with the indicated Delta^{MAX} or SNAG
502 protein. For the CD40-SNAG experiments, the difference was that an equal amount of signal-
503 sending and signal-receiving cells were added same day. Wells without signal-sending cells were
504 used to determine background activation of Notch by Delta^{MAX} and SNAGs. When testing
505 inhibition of endocytosis, 80 μM of the Dynamin inhibitor I (Dynasore, Sigma) was added to the
506 mixture of Notch reporter cells with protein and added to the tissue culture 96-well plate containing
507 the signal-sending cells. Notch activation was measured as previously described.
508
509 **Western blot detection of Notch1 activation by the PDL1-SNAG^{Fc} in MDA-MB-231 cells.**
510 Delta^{MAX} (100 nM protein in 600 mL of DPBS) was non-specifically adsorbed to a single well of a
511 12-well plate for 1 hour at 37 ºC as a positive control for Notch1 activation. The positive control
512 well and three additional wells were then seeded with 200 x 10^3 cells with MDA-MB-231 cells.
513 The plate was centrifuged at 400 x *g* for 4 min to ensure cells were retained at the bottom of each
514 well, and then the media of all wells was discarded. In the first uncoated well, 600 mL of DMEM
515 was added as a negative control. The second well was filled with 600 mL of media containing 100
516 nM of Delta^{MAX}-Fc to monitor Notch1 activation by soluble ligand. The third was filled with 600 mL
517 of media containing 100 nM PDL1-SNAG^{Fc}. The following day, the media was aspirated from all
518 four wells, and the samples were resuspended in 60 mL of Laemli sample buffer with 5% b-
519 mercaptoethanol to lyse cells, followed by boiling at 100 °C for 4 min. Lastly, the samples were
520 analyzed by western blotting using equal protein amounts of cell lysates separated by SDS–PAGE
521 (12% Mini-PROTEAN TGX Precast Protein Gels, Bio-Rad) and transferred to PVDF membranes
522 using an iBlot2 Gel Transfer Device (Thermo Fisher Scientific). The membranes were blocked in
523 3% BSA + 0.1% TBS-Tween. Primary antibodies were anti-Notch1 (D1E11 rabbit mAb, Cell
524 Signaling Technology, 1:1,000), anti-cleaved Notch1 (Val1744 rabbit mAb, Cell Signaling
525 Technology, 1:1,000), and b-actin (rabbit polyclonal Ab, Cell Signaling Technology, 1:1,000).
526 Secondary antibody anti-Rabbit IgG conjugated to HRP (Goat polyclonal Ab, Vector Laboratories,
527 1:8,000) was used for detection of proteins using SuperSignal West Pico PLUS
528 Chemiluminescent Substrate (Thermo Fisher Scientific). Images were acquired using a Chemidoc
529 Imaging System and analyzed with Image-Lab v.6 software (Bio-Rad).
530
531 **Immunofluorescent cell staining.** For endocytosis assays, cells were grown on glass-like
532 polymer bottoms in 24 well black frame plates (Cellvis). For visualization of CD19-SNAG^{Fc} protein
533 binding, 500 nM protein was preincubated with anti-Fc 647 (Alexa Fluor) at 1:200 dilution for 1h
534 on rotation in +4°C. The CD19-SNAG^{Fc}-647 solution was added to cells on ice that were further

535 kept in +4°C for 1 h. For endocytosis, the incubation was followed by washing away non-bound
536 CD19-SNAG^{Fc}-647 with PBS, and 37°C DMEM added to the cells followed by a 15 min incubation
537 in a 37°C incubator. After incubation of CD19-SNAG^{Fc}-647 with or without endocytosis, the cells
538 were fixed in 3% paraformaldehyde and permeabilized with 0.15% Triton X-100 in PBS for 10 min
539 at RT. Nonspecific binding was blocked by incubation in 3% BSA in PBS with 0.05% Triton X-100
540 and 0.1M glycine for 60 min at RT. Cells were further stained for filamentous actin with Alexa 488
541 conjugated to phalloidin (Invitrogen) for 45 min to visualize contours of the individual cells.
542 Hoechst 33342 (Invitrogen) was used to counterstain nuclei. Images were acquired using a
543 Keyence BZ-X710 microscope using a Nikon Plan Apo 20x objective. The far-red channel
544 (magenta) was processed with the de-haze function in the BZ-X710LE analyzer software. A
545 minimum of 100 cells were imaged for each condition.
546
547 **γδ expansion from PBMCs with CD40-SNAG**
548 Peripheral blood mononuclear cells (PBMCs) were isolated from healthy-donor buffy coats using
549 an established density gradient protocol[51]. γδ expansion was performed using zoledronic acid in
550 addition or not of CD40-SNAG. Briefly, ten million cells per condition were resuspended in RPMI
551 [supplemented with 5%FBS, antibiotic, IL-2 (100 IU/ml) and zoledronic acid (4μM)] at 1x106
552 cells/ml. The cells were spiked with CD40-SNAG at three different concentrations (50, 100 or
553 500ng/ml), Delta^{MAX}-Fc (100ng/ml), or CD40L trimer (100ng/ml), and cultured in 24-well plates
554 (2ml/well) for three days at 37C (5% CO2). On day three, the full media was replaced by new
555 media with zoledronic acid and CD40-SNAG, Delta^{MAX}-Fc, or CD40L trimer as on day one. Two
556 days later, cells were lifted from the plates, centrifuged, and resuspended in new RMPI media
557 [5%FBS, antibiotic, IL-2 (100 IU/ml)] without additional molecules. At day seven, T cells were
558 counted, and their phenotype was assessed by surface staining and flow cytometry (using
559 markers for human anti-CD3 – BV711, anti-Vd2 TCR – FITC, anti-CD45RA – BV421, anti-CD27
560 – BV605, and aqua live/dead fluorescent dye).
561
562 **REFERENCES**
563
564 1. Sprinzak, D. & Blacklow, S. C. Biophysics of Notch Signaling. *Annu Rev Biophys* **50**, 157–189
565 (2021).
566 2. Zhou, B. *et al.* Notch signaling pathway: architecture, disease, and therapeutics. *Sig*
567 *Transduct Target Ther* **7**, 1–33 (2022).

568 3. Garg, V. *et al.* Mutations in NOTCH1 cause aortic valve disease. *Nature* **437**, 270–274 (2005).

569 4. Li, L. *et al.* Alagille syndrome is caused by mutations in human Jagged1, which encodes a
570 ligand for Notch1. *Nat. Genet.* **16**, 243–251 (1997).

571 5. Joutel, A. *et al.* Notch3 mutations in CADASIL, a hereditary adult-onset condition causing
572 stroke and dementia. *Nature* **383**, 707–710 (1996).

573 6. Bulman, M. P. *et al.* Mutations in the human delta homologue, DLL3, cause axial skeletal
574 defects in spondylocostal dysostosis. *Nat Genet* **24**, 438–441 (2000).

575 7. Radtke, F. & Raj, K. The role of Notch in tumorigenesis: oncogene or tumour suppressor?
576 *Nat Rev Cancer* **3**, 756–767 (2003).

577 8. Hori, K., Sen, A. & Artavanis-Tsakonas, S. Notch signaling at a glance. *Journal of Cell Science*
578 **126**, 2135–2140 (2013).

579 9. Andersson, E. R. & Lendahl, U. Therapeutic modulation of Notch signalling--are we there
580 yet? *Nat Rev Drug Discov* **13**, 357–378 (2014).

581 10. Brandstadter, J. D. & Maillard, I. Notch signalling in T cell homeostasis and differentiation.
582 *Open Biol* **9**, 190187 (2019).

583 11. Schmitt, T. M. & Zúñiga-Pflücker, J. C. Induction of T Cell Development from Hematopoietic
584 Progenitor Cells by Delta-like-1 In Vitro. *Immunity* **17**, 749–756 (2002).

585 12. Kelliher, M. A. & Roderick, J. E. NOTCH Signaling in T-Cell-Mediated Anti-Tumor Immunity
586 and T-Cell-Based Immunotherapies. *Front Immunol* **9**, 1718 (2018).

587 13. Sierra, R. A. *et al.* Rescue of notch-1 signaling in antigen-specific CD8+ T cells overcomes
588 tumor-induced T-cell suppression and enhances immunotherapy in cancer. *Cancer Immunol*
589 *Res* **2**, 800–811 (2014).

590 14. Wilkens, A. B. *et al.* NOTCH1 signaling during CD4+ T-cell activation alters transcription
591 factor networks and enhances antigen responsiveness. *Blood* **140**, 2261–2275 (2022).
592 15. Kondo, T. *et al.* Notch-mediated conversion of activated T cells into stem cell memory-like T
593 cells for adoptive immunotherapy. *Nat Commun* **8**, 15338 (2017).
594 16. Meloty-Kapella, L., Shergill, B., Kuon, J., Botvinick, E. & Weinmaster, G. Notch ligand
595 endocytosis generates mechanical pulling force dependent on dynamin, epsins, and actin.
596 *Dev. Cell* **22**, 1299–1312 (2012).
597 17. Wang, X. & Ha, T. Defining Single Molecular Forces Required to Activate Integrin and Notch
598 Signaling. *Science* **340**, 991–994 (2013).
599 18. Gordon, W. R. *et al.* Mechanical Allostery: Evidence for a Force Requirement in the
600 Proteolytic Activation of Notch. *Dev. Cell* **33**, 729–736 (2015).
601 19. Rebay, I. *et al.* Specific EGF repeats of Notch mediate interactions with Delta and Serrate:
602 implications for Notch as a multifunctional receptor. *Cell* **67**, 687–699 (1991).
603 20. Luca, V. C. *et al.* Structural biology. Structural basis for Notch1 engagement of Delta-like 4.
604 *Science* **347**, 847–853 (2015).
605 21. Luca, V. C. *et al.* Notch-Jagged complex structure implicates a catch bond in tuning ligand
606 sensitivity. *Science* eaaf9739 (2017) doi:10.1126/science.aaf9739.
607 22. Gordon, W. R. *et al.* Structural basis for autoinhibition of Notch. *Nat. Struct. Mol. Biol.* **14**,
608 295–300 (2007).
609 23. De Strooper, B. *et al.* A presenilin-1-dependent gamma-secretase-like protease mediates
610 release of Notch intracellular domain. *Nature* **398**, 518–522 (1999).

611 24. Brou, C. *et al.* A novel proteolytic cleavage involved in Notch signaling: the role of the
612 disintegrin-metalloprotease TACE. *Mol. Cell* **5**, 207–216 (2000).
613 25. Schroeter, E. H., Kisslinger, J. A. & Kopan, R. Notch-1 signalling requires ligand-induced
614 proteolytic release of intracellular domain. *Nature* **393**, 382–386 (1998).
615 26. Varnum-Finney, B. *et al.* Immobilization of Notch ligand, Delta-1, is required for induction of
616 notch signaling. *J. Cell. Sci.* **113 Pt 23**, 4313–4318 (2000).
617 27. Trotman-Grant, A. C. *et al.* DL4-µbeads induce T cell lineage differentiation from stem cells
618 in a stromal cell-free system. *Nat Commun* **12**, 5023 (2021).
619 28. Li, K. *et al.* Modulation of Notch Signaling by Antibodies Specific for the Extracellular
620 Negative Regulatory Region of NOTCH3. *J. Biol. Chem.* **283**, 8046–8054 (2008).
621 29. Tiyanont, K., Wales, T. E., Siebel, C. W., Engen, J. R. & Blacklow, S. C. Insights into Notch3
622 Activation and Inhibition Mediated by Antibodies Directed Against its Negative Regulatory
623 Region. *J Mol Biol* **425**, 3192–3204 (2013).
624 30. Gonzalez-Perez, D. *et al.* Affinity-matured DLL4 ligands as broad-spectrum modulators of
625 Notch signaling. *Nat Chem Biol* 1–9 (2022) doi:10.1038/s41589-022-01113-4.
626 31. Sprinzak, D. *et al.* Cis-interactions between Notch and Delta generate mutually exclusive
627 signalling states. *Nature* **465**, 86–90 (2010).
628 32. Cordle, J. *et al.* A conserved face of the Jagged/Serrate DSL domain is involved in Notch
629 trans-activation and cis-inhibition. *Nat Struct Mol Biol* **15**, 849–857 (2008).
630 33. Braun, M. B. *et al.* Peptides in headlock – a novel high-affinity and versatile peptide-binding
631 nanobody for proteomics and microscopy. *Sci Rep* **6**, (2016).

632 34. Andersson, E. R. *et al.* Mouse Model of Alagille Syndrome and Mechanisms of Jagged1
633 Missense Mutations. *Gastroenterology* **154**, 1080–1095 (2018).
634 35. Lafkas, D. *et al.* Therapeutic antibodies reveal Notch control of transdifferentiation in the
635 adult lung. *Nature* **528**, 127–131 (2015).
636 36. Powles, T. *et al.* MPDL3280A (anti-PD-L1) treatment leads to clinical activity in metastatic
637 bladder cancer. *Nature* **515**, 558–562 (2014).
638 37. Xiao, D. *et al.* Development of bifunctional anti-PD-L1 antibody MMAE conjugate with
639 cytotoxicity and immunostimulation. *Bioorganic Chemistry* **116**, 105366 (2021).
640 38. Zammarchi, F. *et al.* ADCT-402, a PBD dimer-containing antibody drug conjugate targeting
641 CD19-expressing malignancies. *Blood* **131**, 1094–1105 (2018).
642 39. Lewis Phillips, G. D. *et al.* Targeting HER2-positive breast cancer with trastuzumab-DM1, an
643 antibody-cytotoxic drug conjugate. *Cancer Res* **68**, 9280–9290 (2008).
644 40. Parks, A. L., Klueg, K. M., Stout, J. R. & Muskavitch, M. A. Ligand endocytosis drives receptor
645 dissociation and activation in the Notch pathway. *Development* **127**, 1373–1385 (2000).
646 41. Koo, B.-K. *et al.* An obligatory role of mind bomb-1 in notch signaling of mammalian
647 development. *PLoS One* **2**, e1221 (2007).
648 42. McMillan, B. J. *et al.* A tail of two sites: a bipartite mechanism for recognition of notch
649 ligands by mind bomb E3 ligases. *Mol Cell* **57**, 912–924 (2015).
650 43. Cao, R. *et al.* Structural requirements for activity of Mind bomb1 in Notch signaling.
651 *Structure* (2024) doi:10.1016/j.str.2024.07.011.

652 44. Yellin, M. J. *et al.* CD40 molecules induce down-modulation and endocytosis of T cell surface
653 T cell-B cell activating molecule/CD40-L. Potential role in regulating helper effector function.
654 *J Immunol* **152**, 598–608 (1994).
655 45. Mitchison, N. A. T-cell–B-cell cooperation. *Nat Rev Immunol* **4**, 308–312 (2004).
656 46. Naito, M. *et al.* CD40L-Tri, a novel formulation of recombinant human CD40L that effectively
657 activates B cells. *Cancer Immunol Immunother* **62**, 347–357 (2013).
658 47. Mensurado, S., Blanco-Domínguez, R. & Silva-Santos, B. The emerging roles of γδ T cells in
659 cancer immunotherapy. *Nat Rev Clin Oncol* **20**, 178–191 (2023).
660 48. Ganapathy, T., Radhakrishnan, R., Sakshi, S. & Martin, S. CAR γδ T cells for cancer
661 immunotherapy. Is the field more yellow than green? *Cancer Immunol Immunother* **72**, 277–
662 286 (2023).
663 49. Frieling, J. S. *et al.* γδ-Enriched CAR-T cell therapy for bone metastatic castrate-resistant
664 prostate cancer. *Sci Adv* **9**, eadf0108.
665 50. Gogoi, D., Dar, A. A. & Chiplunkar, S. V. Involvement of Notch in activation and effector
666 functions of γδ T cells. *J Immunol* **192**, 2054–2062 (2014).
667 51. Peters, C., Kouakanou, L., Oberg, H.-H., Wesch, D. & Kabelitz, D. *In vitro* expansion of Vγ9Vδ2
668 T cells for immunotherapy. in *Methods in Enzymology* (eds. Galluzzi, L. & Rudqvist, N.-P.) vol.
669 631 223–237 (Academic Press, 2020).
670 52. Liu, Q., Sun, Z. & Chen, L. Memory T cells: strategies for optimizing tumor immunotherapy.
671 *Protein Cell* **11**, 549–564 (2020).

672 53. Medina, E., Perez, D. H., Antfolk, D. & Luca, V. C. New tricks for an old pathway: emerging
673 Notch-based biotechnologies and therapeutics. *Trends Pharmacol Sci* S0165-
674 6147(23)00213–4 (2023) doi:10.1016/j.tips.2023.09.011.
675 54. Bonnici, L., Suleiman, S., Schembri-Wismayer, P. & Cassar, A. Targeting Signalling Pathways in
676 Chronic Wound Healing. *International Journal of Molecular Sciences* **25**, 50 (2024).
677 55. Mazor, Y. *et al.* Enhanced tumor-targeting selectivity by modulating bispecific antibody
678 binding affinity and format valence. *Sci Rep* **7**, 40098 (2017).
679 56. Haber, L. *et al.* Generation of T-cell-redirecting bispecific antibodies with differentiated
680 profiles of cytokine release and biodistribution by CD3 affinity tuning. *Sci Rep* **11**, 14397
681 (2021).
682 57. del Álamo, D., Rouault, H. & Schweisguth, F. Mechanism and Significance of cis-Inhibition in
683 Notch Signalling. *Current Biology* **21**, R40–R47 (2011).
684 58. Boyd, N. *et al.* 'Off-the-Shelf' Immunotherapy: Manufacture of CD8+ T Cells Derived from
685 Hematopoietic Stem Cells. *Cells* **10**, 2631 (2021).
686 59. Tan, W. K., Tay, J. C., Zeng, J., Zheng, M. & Wang, S. Expansion of Gamma Delta T Cells - A
687 Short Review on Bisphosphonate and K562-Based Methods. *Journal of Immunological*
688 *Sciences* **2**, (2018).
689 60. Verkerk, T. *et al.* Isolation and expansion of pure and functional γδ T cells. *Front. Immunol.*
690 **15**, (2024).
691 61. Xu, X. *et al.* Insights into Autoregulation of Notch3 from Structural and Functional Studies of
692 Its Negative Regulatory Region. *Structure* **23**, 1227–1235 (2015).

693 62. Smyrlaki, I. *et al.* Soluble and multivalent Jag1 DNA origami nanopatterns activate Notch
694 without pulling force. *Nat Commun* **15**, 465 (2024).
695 63. Abanades, B. *et al.* The Patent and Literature Antibody Database (PLAbDab): an evolving
696 reference set of functionally diverse, literature-annotated antibody sequences and
697 structures. *Nucleic Acids Research* **52**, D545–D551 (2024).
698